

A magnetic field diagnostic for sonoluminescence

Tom Chou¹ and Eric G. Blackman²

¹*LASSP, Cornell University, Ithaca, NY 14853*

²*Institute of Astronomy, Cambridge University, Madingley Road, Cambridge CB3 0HA, England*
(July 13, 2021)

This study is motivated by the extraordinary process of single bubble sonoluminescence (SBSL), where an acoustically driven spherical shock is thought to power the emitted radiation. We propose new experiments using an external magnetic field which can induce anisotropies in both the shock propagation and radiation pattern. The effects will depend on the temperature, conductivity, and size of the radiating region. Our predictions suggest that such a laboratory experiment could serve as an important diagnostic in placing bounds on these parameters and understanding the physics of sonoluminescence.

Sonoluminescence, first discovered in 1933 [1,2], is a remarkable phenomenon whereby sound is converted into light. Recently, the process involving a single small gas bubble trapped in a degassed liquid such as water, which is then acoustically driven, has been studied [3]. Since the sound wavelength is much larger than the bubble radius $R(t)$, (see Fig. 1), the bubble feels a uniform pressure which varies with time. The gas bubble then undergoes complicated nonlinear oscillations. At a threshold of the driving pressure of about 1.15 atm, short (< 50 ps), intense pulses of light are radiated. The acoustic energy of the system is thus focused into a small region within the bubble for very short times. Recent interest in sonoluminescence has been in part motivated by possible technological applications in biophysics, sonochemistry and reactions at ultra-high temperatures [4].

Experiments have probed the effects of ambient temperature, liquid composition, gas composition, driving intensity, and frequency on the phenomenon. In the experiments of Ref. [3], there appears to be a sharp transition from a nonradiating oscillating bubble to a luminescing one. Spectral fits to blackbody or Bremsstrahlung emission are inconclusive but suggest temperatures of at least 5000°K [3,4].

Theoretical attention has focused on bubble dynamics, usually employing variations of the Rayleigh-Plesset equation to model the bubble motion and stability [3,5]. Furthermore, studies imply that as the gas bubble shrinks, it launches an inwardly propagating shock wave [6]. The shock collapses to the center, rebounds, and can hit the liquid/gas bubble wall from which it was launched. Radiation is thought to be emitted immediately after the shock rebounds from the center, where extremely high temperatures and ionization are predicted [6]. Numerical simulations suggest temperatures of 10^8 °K [6], much higher than those implied by experiments. Thermal blackbody and/or Bremsstrahlung radiation, Casimir effects, [7] or decay of excited molecular states, have all been suggested as relevant processes involved in the luminescence, but the emission spectra in SBSL are so featureless that distinguishing among radiation mechanisms is difficult. Despite attention on the effects of bubble dynamics, diffusion, and material composition on sonoluminescence, our understanding of the underlying physical mechanisms remains an unsorted mixture of nonlinear hydrodynamics, shock physics and chemical reaction kinetics. However, one emerging criterion for SBSL is the necessity of stability of spherical symmetry in bubble structure $R(t)$ [8]. The transient symmetric stability of the converging shock is also thought to be crucial for SBSL.

In this Letter, we suggest the use of an externally applied magnetic field as a diagnostic by catalyzing the breaking of spherical stability and putting bounds on the temperature, conductivity, and ionization of the sonoluminescing bubble. The external magnetic field can break spherical symmetry of the shock, bubble, or radiation patterns and disrupt or alter sonoluminescent behavior.

Effects of \vec{B} on bubble structure - We assume that the bubble gas is ionized at some point in the acoustic cycle. Adiabatic compression of the gas bubble $R(t)$ is probably sufficient to partially ionize the gas; Saha's equation for temperatures of 7000°K give roughly 5% ionization. First consider the possibility that during the adiabatic collapse, a spherical region of plasma has a high conductivity σ_p such that the magnetic Reynolds number $R_M = \sigma_p v R^* \gg 1$ (where v, R^* are typical velocities and the radius of the ionized region). Alfvén's theorem of flux freezing holds, and the application of \vec{B}_{ext} adds an magnetic stiffness in the direction perpendicular to \vec{B}_{ext} . The ionized region then collapses asymmetrically, with the poles compressing more than the equator. If $R_M \gg 1$ is not achieved by initial adiabatic compression, shocks launched by the liquid/gas interface may further compress, heat, and ionize the plasma, consistent with numerical simulations [6].

Shocks form when the hydrodynamic velocity exceeds a characteristic group velocity. In the presence of a magnetic field, characteristic group velocities depend on the magnitude and orientation of the applied field. For $R_M \gg 1$, the

MHD modes have group velocities [9]

$$v^2 = \frac{1}{2}(c_s^2 + v_A^2) \pm \frac{1}{2}\sqrt{(c_s^2 + v_A^2)^2 - 4c_s^2 v_A^2 \cos^2 \theta} \quad (1)$$

and $v = v_A \cos \theta$, where $v_A^2 = B^2/(4\pi\rho)$ and c_s is the hydrodynamic sound speed (B is the magnetic field in the region of interest and ρ is the plasma density). These are the magneto-acoustic waves and the Alfvén wave respectively. The angular dependence of these velocities will break the spherical symmetry of a plasma shock.

We consider a shock just after rebound since here the upstream region was previously shocked during pre-rebound and more likely to be in a high R_M state. We will first assume $R_M \gg 1$ both upstream and downstream. (The possibly important but rather involved case of ionizing shocks will not be treated here.) The governing equations are the mass, momentum, and energy conservation, and the steady state Maxwell's equations and Ohm's law, $\vec{E} \simeq c/(4\pi\sigma)\nabla \times \vec{B} - (\vec{v}/c) \times \vec{B}$, valid for $\omega_B^{-1} = m_e c/eB_0 < \text{collision time}$ (c, m_e, e are the speed of light, electron mass, and electron charge respectively). Locally integrating the conservation laws perpendicular to a shock, these equations are $\nabla \cdot \vec{B} = \nabla \cdot (\rho\vec{v}) = 0$ and, [10]

$$\begin{aligned} \eta \hat{n} \times \nabla \times \vec{B} &= \left[\hat{n} \times (\vec{v} \times \vec{B}) \right]_0^x, \\ \rho\nu (\hat{n} \cdot \nabla v_i + \frac{1}{3}n_i \nabla \cdot \vec{v}) &= \left[(\vec{B} \cdot \vec{n})B_i/4\pi - \rho v_i (\vec{v} \cdot \vec{n}) - P_M n_i \right]_0^x, \\ \frac{\eta}{4} \hat{n} \cdot (\nabla \times \vec{B}) \times \vec{B} &= \left[\hat{n} \cdot \vec{v} (u + \frac{1}{2}\rho v^2 + P_M) - \frac{1}{4\pi} (\vec{B} \cdot \vec{v}) (\vec{B} \cdot \hat{n}) \right]_0^x, \end{aligned} \quad (2)$$

where $[S]_0^x \equiv S(x) - S(0)$ and $u = P/(\gamma - 1)\rho$ is the internal energy of the gas (P, η , and $\gamma = C_p/C_v$ are the pressure, shear viscosity and adiabatic index of the gas, respectively). The limits straddling the shock are far outside the shock bubble (0), where all quantities are uniform, and x , a normal distance downstream. The total pressure $P_M \equiv P + B^2/8\pi$ (for $R_M \gg 1$, the E^2 contribution is smaller than B^2 by $(v/c)^2$, which is small; for $R_M \ll 1$, E^2 is smaller by $(v/c)^2/R_M$). Equations (2) include dissipation due to plasma shear viscosity ν and resistivity $\eta \equiv c^2/(4\pi\sigma)$. We can neglect the contribution of the any short intense radiation burst to the electromagnetic stress tensor if we focus only on the shock conditions just before or after the radiative burst. Compression ratios and pressure jumps depend on θ , the angle between the \vec{B}_0 and the shock normal. We thus expect a nonuniform MHD shock forming first at the poles where $\theta = 0$ and B_0 offers no additional stiffness.

In the high conductivity ($R_M \rightarrow \infty$) limit, all quantities vary over a thin shock front such that the fields at $x = 0^-$ are uniform and gradient terms vanish when we consider the quantities away from the sharp transition region. Upon solving the resulting equations (Rankine-Hugoniot) we obtain,

$$\begin{aligned} \beta [\gamma M_0^2(1 - 1/s) - \Delta + 1] &= (\alpha^2 - 1) \sin^2 \theta \\ \frac{2\gamma}{\gamma - 1} \left(\frac{\Delta}{s} - 1 \right) + \gamma M_0^2 \left(\frac{1}{s^2} - 1 \right) &= 4\beta^{-1}(1 - \alpha) \sin^2 \theta - \gamma M_0^2 \tan^2 \theta \left(1 - \frac{\alpha}{s} \right)^2 \end{aligned} \quad (3)$$

where $\alpha \equiv (\beta\gamma M_0^2 - 2\cos^2 \theta)/(\beta\gamma M_0^2/s - 2\cos^2 \theta)$, $\beta = 8\pi P_0/B_0^2$ is the ratio of the particle to magnetic pressure, and $M_0 = u_0/c_s$ is the Mach number. The roots of Eqs. (3), s and $\Delta (> 1)$, determine the thermodynamically allowed shock states.

Fig. 2 shows the local shock structure for $\gamma = 5/3$ and at varying M_0 and β . Except for low β and M_0 , the compression and density ratios, Δ and s , incur their greatest jumps at the poles. Numerically predicted pressures are on the order 10^{10} dyne/cm² [6], thus, fields of $B_0 \sim 10$ T are required for $\beta \approx O(1)$. The angle θ can more or less be associated with the angle of \vec{B}_{ext} in Fig. 1. Deformations of the ionized region before shock formation will stretch the x -axes in Fig. 2 depending on β . Fig. 2, however, shows the difference in jumps between $\theta = 0, \pi/2$. For large β , the shock will be nearly spherical, but magnetic field compression near the equator would tend to decrease θ throughout the hemisphere. When β is small, the shock surface will be oblate owing to the lateral magnetic stiffness, and again, smaller θ will approximate most of the surface. In fact, the shock solution ends at a switch-off shock for low enough β . Dissipative processes will smear this region.

In the limit $R_M \rightarrow 0$ (low conductivity, or small velocity or length scales) the magnetic field and the plasma flow are decoupled, and the plasma can slide freely through the field. The discontinuities in s, Δ and \vec{v} approach those of a hydrodynamic shock and the effect of the external \vec{B} -field for $R_M \ll 1$ is expected to be small. Though the result given by (3) is correct for all R_M , for small R_M the \vec{B} -field dissipation length L becomes much larger than the viscous dissipation length δ – the scale over which pressure and velocity vary.

Instead of solving the nonlinear differential equations (2) [10], we simply estimate the variation of B across δ at $\theta = \pi/2$, where the largest effect occurs. Most of the variation in \vec{v}, ρ , and P will occur over δ ; far enough away

from the shock the differences in the uniform states (0 and 1) are given by (3). Using $dB/dx \simeq (B_0 - B_1)/L$, and evaluating quantities in Eqs. (2) across δ , s and Δ to order R_M/β are

$$\begin{aligned} s &= \bar{s} - 2 \frac{(M_0^2(\gamma - 1) - \gamma)^2 + M_0^2\gamma(\gamma - 1)}{(M_0^2(\gamma - 1) + \gamma)^2} \left(\frac{R_M}{\beta} \right) f(\theta) \\ \Delta &= \bar{\Delta} - \frac{2\gamma}{M_0^2} \left(\frac{4M_0^2\gamma}{\gamma - 1} - \frac{3\gamma + 1}{\gamma - 1} \right) \left(\frac{R_M}{\beta} \right) g(\theta), \end{aligned} \quad (4)$$

where $\bar{s} = (\gamma + 1)M^2/(\gamma + M_0^2(\gamma - 1))$ and $\bar{\Delta} = (4M_0^2 - \gamma + 1)/(\gamma + 1)$ are the density and compression ratios of a pure hydrodynamic shock. The angular dependences obey $f(0) = g(0) = 0$ and $f(\pm\pi/2) = g(\pm\pi/2) = 1$. As expected, the shock anisotropy is small if R_M/β is small.

Effects of \vec{B} on radiation - Even when \vec{B}_{ext} does not alter the shock structure, it can have other effects on SBSL. We now consider the effects on the SBSL radiation. Shock simulations suggest maximum temperatures of $\sim 10^8$ °K [6] while spectral fits from radiation emanating from the bubble center suggest a more modest $\sim 10^4$ °K [4]. The average thermal velocity at these temperatures is $< 0.1c$, hence, we will only consider the nonrelativistic conditions for observing anisotropic cyclotron radiation in competition with isotropic Bremsstrahlung or blackbody emission. We ignore collective effects and thus require $\omega_B > \omega_p$, the plasma frequency. For appropriately dense plasmas, $\omega_p \approx 10^{11} - 10^{12}$ /s, requiring $B_0 > 1 - 10$ T.

If shock asymmetry is negligible (*e.g.* if $R_M \ll 1$), then the plasma feels the externally applied magnetic field $\vec{B}_0 \simeq B_{ext}\hat{z}$ and charge trajectories obey $\dot{\mathbf{v}}_e = (e/m_e)\mathbf{v}_e \times \vec{B}_0$, where \mathbf{v}_e is the electron velocity. The dipole approximation for cyclotron emission power per unit solid angle of a collection of uncorrelated electrons is given by [11]

$$dL_c/d\Omega \simeq (n_e e^2/4\pi c^3)(\hat{n} \times (\hat{n} \times \dot{\mathbf{v}}_e))^2 = (n_e e^4/4\pi m_e^2 c^5)v_\perp^2 B_0^2(1 - \sin^2\theta \sin^2\varphi) \quad (5)$$

where n_e is the ionized electron density, \hat{n} is in the direction of the observer, θ is the angle between the field and the line of sight, and φ is the azimuthal angle to be averaged over. Note that for $\omega_B^{-1} \ll 50$ ps, also requires $B_0 > 1 - 10$ T.

To get the integrated power as a function of θ , we average over the uncorrelated \mathbf{v}_e using $f(v_e, x, t)d^3\mathbf{v}_e = \exp[-v_T^{-2}(v_\perp^2 + v_z^2)]v_\perp dv_\perp dv_z d\varphi$, where $v_T \equiv (2k_B T/m_e)^{1/2}$. We also impose a cutoff on the velocity, $v_z, v_\perp < \ell_c \omega_B$, where $\ell_c = \min\{\lambda, R^*\}$, $\lambda = 4k_B^2 T^2/n_e e^4$, is the mean free path for electron collisions, and R^* is the size of the ionized region. This ensures that the charge can coherently twist around the magnetic field sufficiently to radiate near ω_B . The cyclotron power is then

$$L_c(\theta) = n_e(e^4 B_0^2 v_T^2/8\pi m_e^2 c^5) [1 - (\Lambda + 1)e^{-\Lambda}] \text{Erf}(\sqrt{\Lambda})(1 + \cos^2\theta), \quad (6)$$

where $\Lambda \equiv (\ell_c \omega_B)^2 m/2k_B T$. When $\ell_c = \lambda < R_c$, $\Lambda \propto T^3$, but when $\ell_c = R_c < \lambda$, $\Lambda \propto 1/T$. Thus the maximum range of v_\perp, v_z contributing to L_c would occur where $\lambda \simeq R_c$. When $\Lambda \gg 1$, $L_c(\theta) = n_e(e^4 v_T^2 B_0^2/16\pi m_e^2 c^5)(1 + \cos^2\theta)$, the standard expression [9]. When $\Lambda \ll 1$,

$$L_c(\theta) \simeq n_e(v_T^2 \pi)^{-3/2} \left(\frac{e^2}{8c} \right) \ell_c^5 \omega_B^7 (1 + \cos^2\theta) + O(\Lambda^{7/2}). \quad (7)$$

To determine when anisotropic emission may be observable, we compare the cyclotron intensities with those from isotropic Bremsstrahlung and blackbody emissions. We consider a singly ionized species in a neutral plasma, justified because the Debye length $\ll R^*$. Near ω_B , the isotropic Bremsstrahlung radiation power in the dipole approximation is,

$$L_{brem}(\omega_B) \simeq \int_{\omega_B - \Gamma/2}^{\omega_B + \Gamma/2} d\omega \frac{dL_{brem}(\omega)}{d\omega} \simeq \frac{16n_e^2 e^6}{3c^3 m_e^2} (v_T^2 \pi)^{-1/2} \ell_n \left(\frac{v_T^2}{\omega^2 b_{min}^2} \right) \Gamma \quad (8)$$

where $b_{min} \sim 4e^2/\pi m_e v_T^2$ is a minimum impact parameter, and where Γ is the cyclotron line width or the narrow bandwidth of a detector. Detector bandwidths can be made very narrow ($< 1\text{cm}^{-1}$), so we use $\Gamma \simeq \omega_{col} \sim (2k_B T/m_e \lambda^2)^{1/2} \sim 7 \times 10^{12} (n_e/10^{22})(T/10^6\text{K})^{-3/2} \text{s}^{-1}$ from collisional broadening, which dominates Doppler broadening for $T < 10^8\text{K}$. (We have assumed the neutral plasma to have a density $\sim 10^7\text{kg/m}^3$ consisting primarily of singly ionized nitrogen.) The power radiated by a blackbody at low frequencies (for $B = 10\text{T}$, ω_B is in the IR/microwave region $\simeq 1.8 \times 10^{12}/\text{s}$) is $L_{bb}(\omega_B) \simeq \Gamma \omega_B^2 k_B T/(\pi^2 c^3) \sim 10^{-3} (\omega_B/1.3 \times 10^{13} \text{sec}^{-1})^2 (T/10^6\text{K}) (\Gamma/7 \times 10^{12} \text{sec}^{-1}) \text{erg/sec}$. Similarly, $L_{brem} \sim 6.4 \times 10^{14} (n_e/10^{22} \text{cm}^{-3})^2 (T/10^6\text{K})^{-1/2} (\Gamma/7 \times 10^{12} \text{sec}^{-1}) \text{erg/sec}$, where the Gaunt factor logarithm in (8) is ~ 1 . Now $\Lambda \sim 10^{-4}$, for these characteristic parameters, and $L_c \sim 6 \times 10^{26} (n_e/10^{22} \text{cm}^{-3}) (\omega_B/1.3 \times$

$10^{13}\text{sec}^{-1})^7(\ell_c/10^{-6}\text{cm})^5(T/10^6\text{K})^{-3/2}\text{erg/sec}$ so L_c will dominate. In this estimate we have taken $\ell_c \sim R^*$. Note that the dominance of L_c depends strongly on ω_B .

Discussion - We have illustrated how a magnetic field \vec{B}_{ext} may break the symmetry of a collapsing ionized region or a propagating shock (Fig. 2) in two limits of R_M . Using Spitzer's formula to estimate σ_p at 10^8K and typical velocity and length scales from shock simulations [6], we conservatively estimate $R_M \approx 10^{-3}$. However, in general, consider Guderly's solution [12] for a spherical hydrodynamic shock: $r(t) \propto t^n$, where $t = 0$ is the time the imploding shock collapses. Here, $v(t) \propto t^{n-1}$, and $R_M \simeq \sigma_p t^{2n-1}$. For noninteracting gases, $n > 1/2$, implying $R_M \rightarrow 0$ as the shock converges ($t \rightarrow 0$) and rebounds. It is possible that $n < 1/2$ for compressed materials with large $\gamma = C_p/C_v$. Experiments using gases that have $n < 1/2$ when compressed and heated, if they exist, would be in the $R_M \rightarrow \infty$ regime, where shocks will be strongly perturbed by \vec{B}_{ext} (Fig. 2).

In either case, large or small R_M , anisotropies develop during the evolution of a shock. These anisotropies are greater for smaller β (larger B_0), but vanish as $R_M/\beta \rightarrow 0$. Spherically converging hydrodynamic shocks are inherently unstable. If luminescence requires a spherically converging shock, \vec{B}_{ext} may further destabilize the shock leading to reduced heating upon implosion and destroy luminescence. Comparison of experiments with numerical results can then produce an estimate of R_M . Furthermore, the θ -dependent pressure exerted on the liquid/gas interface by a recolliding shock may destabilize the nonlinear bubble oscillations. An external magnetic field can thus indirectly alter the region of bubble oscillation stability [8]. It is thought that bubble stability is crucial for SBSL. Experiments with external fields can determine the relative importance of symmetric shocks for radiation phenomenon and stable bubble oscillations in SBSL. Differences between multiple bubble sonoluminescence (MBSL) and SBSL can also be probed; if only SBSL depends strongly on symmetric bubble oscillations, an external field would affect SBSL and not MBSL.

For low R_M , especially with strong magnetic fields, the radiation can be expected to have an anisotropic cyclotron component given by (6). Experimental determination of the luminescing spectrum is interrupted by the surrounding water which cuts out light with wavelength below ~ 220 nm. We therefore suggest that structure may be observed at *longer* IR and microwave wavelengths, near ω_B and its higher harmonics. An angular dependence of the form $\sim 1 + \cos^2 \theta$ may be observed if enough signal can be collected from a narrow bandwidth detector set at $n\omega_B$. Given the stable, oscillatory nature of SBSL, this seems feasible. One may be able to discern structure at these harmonics by comparing the complicated low frequency spectra with and without \vec{B}_0 . It is straightforward to estimate the cyclotron contribution by comparing $L_c/(L_c + L_{brem} + L_{bb})$ at $\theta = 0$ and $\pi/2$ using (6) and (8). If no effects are observed with strong \vec{B}_{ext} , the interpretation depends on the optical depth: If the plasma were optically thick, blackbody would be the only emission mode. If the plasma were optically thin, the absence of cyclotron emission means that the velocity cutoff determined by Λ would be very small because $\omega_{col} \gg \omega_B$. L_{brem} would therefore dominate. Since L_{brem} and L_{bb} differ by many orders of magnitude near ω_B , the two cases should be distinguishable. Radiation anisotropy may be detected at low R_M .

The spectroscopy of a sonoluminescing bubble in a magnetic field can help put bounds on relevant physical parameters such as charge density, and temperature. In particular, $L_c \propto T^{-3/2}$ when $\ell_c \simeq R^* < \lambda$, but $L_c \propto T^{17/2}$ when $\ell_c \simeq \lambda < R^*$. The temperature when $R^* = \lambda$, above which $L_c \propto T^{-3/2}$, is given by $T_{crit} \sim 10^5(R_c/10^{-6}\text{cm})^{1/2}(n_e/10^{22}\text{cm}^{-3})^{1/2}\text{K}$. Since increasing the acoustic driving pressure increases T , the functional change in L_c (anisotropy) could help constrain T . Finally, note that experiments hitherto have time-integrated the radiation. A time dependent spectral analysis of asymmetric radiation near ω_B can be a means of monitoring the temperature and charge density of the heat-up and cool-down phases of the bubble oscillation, in addition to the 50ps burst. Experiments of this nature may help clarify the mechanisms involved in sonoluminescence.

T.C. thanks M. Brenner and R.V.E. Lovelace for helpful discussions and N. Kannan for assistance in plotting Fig. 2(a).

-
- [1] N. Marinesco and J. J. Trillat, C.r. hebdom. Seanc. Acad. Sci., Paris, **196**, 858, (1933); H. Frenzel and H. Schultes, Z. phys. Chem., **27b**, 421, (1934).
 - [2] A. J. Walton and G. T. Reynolds, Adv. Phys., **33**(6), 595, (1984)
 - [3] D. F. Gaitan, L. A. Crum, C. C. Church, and R. A. Roy, J. Acoust. Soc. Am. **91**, 3166, (1992); R. Lofstedt, B. Barber, and S. Putterman, Phys. Fluids, **A5**(11), 2911, (1993); W. C. Moss, D. B. Clarke, J. W. White, and D. A. Young, Phys. Fluids, **6**(9), 2979, (1994)

- [4] K. S. Suslick, *Science*, **247**, 1439, (1990)
- [5] H. P. Greenspan and A. Nadim, *Phys. Fluids A***5**(4), 1065, (1993)
- [6] C. C. Wu and P. H. Roberts, *Phys. Rev. Lett.*, **70**, 3424, (1993); C. C. Wu and P. H. Roberts, *Proc. R. Soc. Lond. A***445**, 323, (1994)
- [7] J. Schwinger, *Proc. Natl. Acad. Sci., USA*, **89**, 1118, 4091, (1992)
- [8] M. P. Brenner, D. Lohse, and T. F. Dupont, *Phys. Rev. Lett.*, **75**(5), 954, (1995)
- [9] T. J. M. Boyd and J. J. Sanderson, *Plasma Dynamics*, (Barnes & Noble, New York, 1969)
- [10] W. Marshall, *Proc. Roy. Soc.*, **233**, 367, (1956)
- [11] J.D. Jackson, *Classical Electrodynamics*, 2nd Ed., (John Wiley & Sons, New York, 1975)
- [12] G. B. Whitham, *Linear and Nonlinear Waves*, (John Wiley & Sons, New York, 1973)

FIG. 1. The sonoluminescing bubble in an external magnetic field $B_0\hat{z}$. The liquid/gas interface and the shock front are denoted by $R(t)$ and $r(t)$ respectively. The external sound field supplies the pressure P_a .

FIG. 2. The pressure and density ratios for $R_M \gg 1$. (a) Δ as a function of θ for $M_0 = 1.5$ (lower 3 thin curves), and $M_0 = 3$ (upper 3 thick curves). Solid, dotted, and dashed curves correspond to $\beta = 10, 1, 0.1$, respectively. (b) Density ratio s for similar values of M_0 and β .

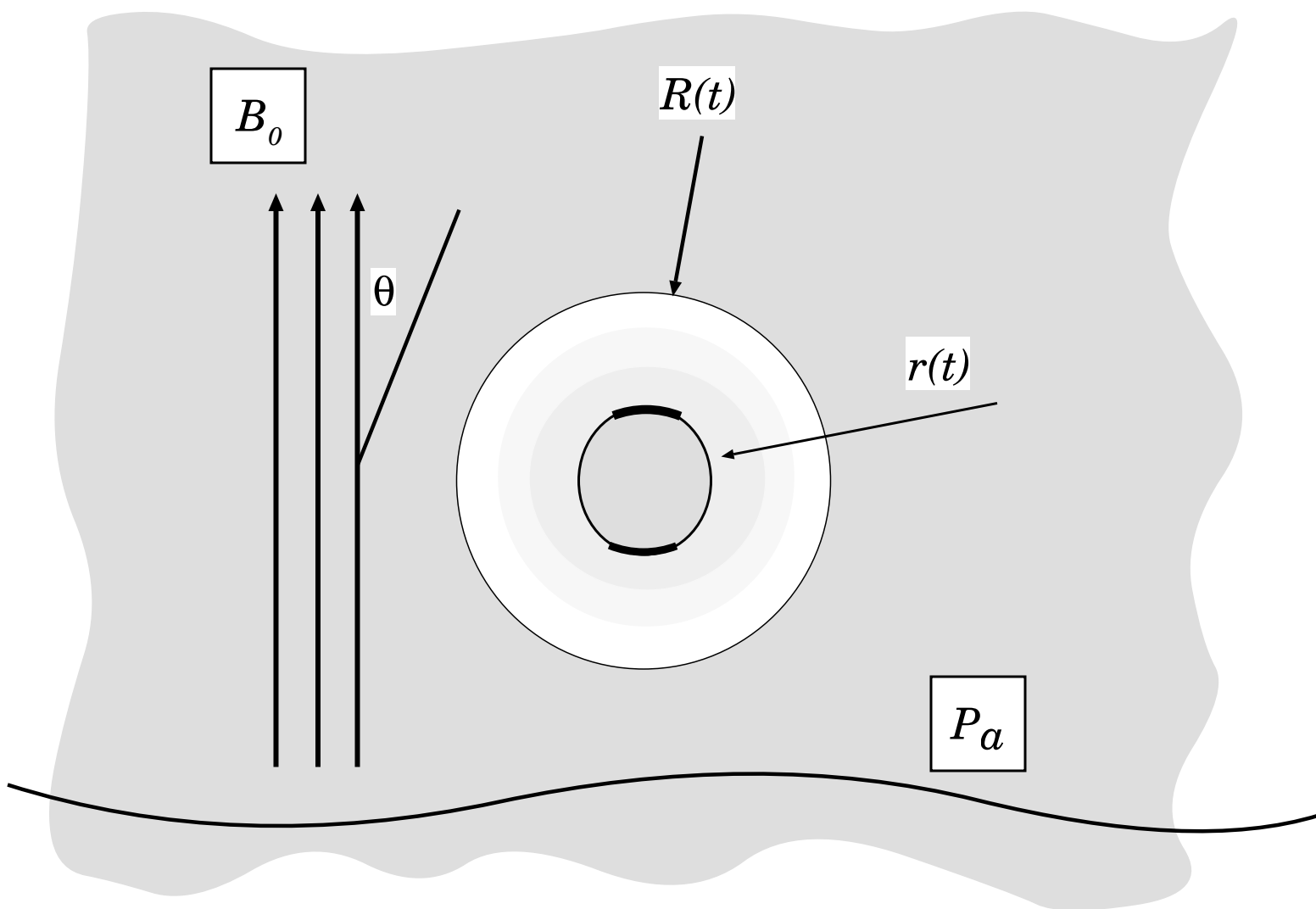


Figure 1

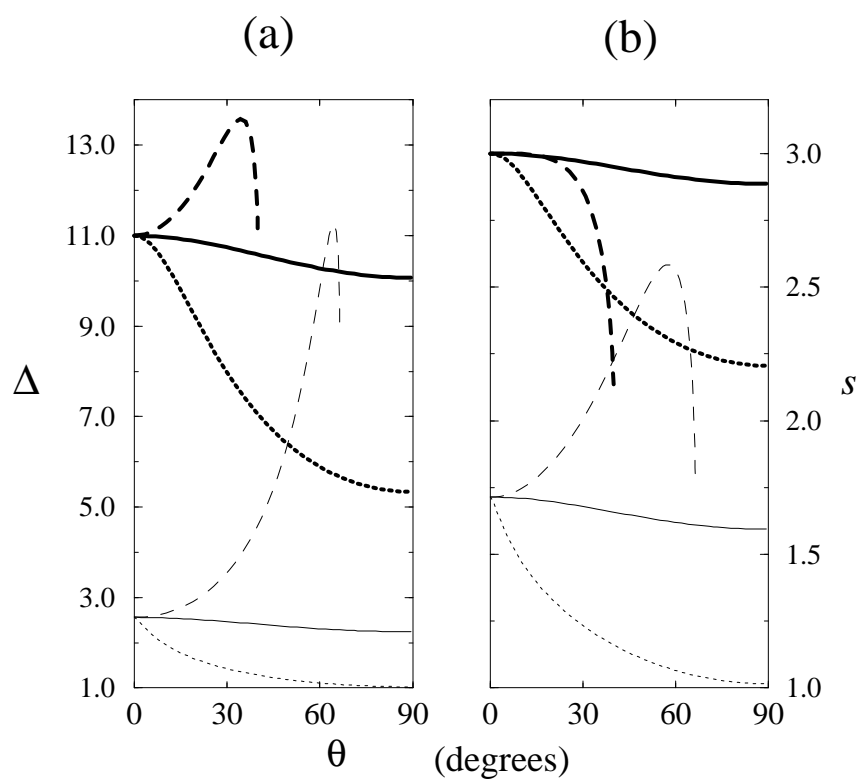


Figure 2